ENGINEERING

A basal-bolus insulin regimen integrated microneedle patch for intraday postprandial glucose control

Bo Zhi Chen, Li Qin Zhang, Yi Yun Xia, Xiao Peng Zhang, Xin Dong Guo*

Multiple daily insulin injections have been a common regimen worldwide for the management of diabetes mellitus but involved potential safety and compliance problems. In this context, a single integrated microneedle patch (IMP) with multiple release kinetics is demonstrated to provide better physiologic insulin coverage for postprandial glycemic excursion in a convenient and pain-free manner. The combination of rapid separating technique and multiple individual microneedle arrays provides the combined ability to efficiently deliver insulin into the skin within seconds and to independently control insulin release kinetics. In addition, the diabetic rats with a traditional breakfast-lunch-dinner lifestyle exhibit obvious intraday glucose fluctuations, while the hypoglycemic experiments indicate that the IMP is capable of simultaneous bolus and sustained insulin delivery to closely match the glucose rise that occurs in response to meals and efficiently minimize excessive fluctuations, suggesting the potential of this new transdermal insulin delivery system as substitutes for multiple daily injections.

INTRODUCTION

Optimal treatment of diabetes mellitus generally requires intensive insulin therapy to achieve effective glycemic control and to reduce late complications (*1*). Multiple daily insulin injections remain the common mode of administration so far due to the short half-life and enzymatic degradation of insulin in the gastrointestinal tract (*2*). However, frequent glucose monitoring and painful injections associated with this treatment regime often lead to poor patient compliance and may cause upsetting side effects. Other concerns include hazardous waste disposal and unsafe injection practices in certain countries as a source of blood-borne pathogens (*3*). These invasiveness and discomfort, in a sense, directed exploitations in insulin therapy to alternative nonparenteral delivery systems that are less invasive and lack of pain (*4*). The emergence of nasal delivery provides a noninvasive and painless solution; various forms of commercially available insulin are being atomized into a spray and inhaled through the nose. The main limitations, however, of current intranasal insulin are the mucociliary clearance mechanism and the active proteolytic enzymes that lower the bioavailability and increase the variability of delivered insulin (*5*). One highlight of recent efforts is the development of a microneedle (MN) patch, which is capable of effectively overcoming the inherent barriers for insulin uptake across the skin and thus promoting transdermal drug delivery without external energy sources or complex systems.

MN system is based on the miniaturization of multiple needles within a patch to the micrometer dimensions (less than 1 mm in length) that painlessly pierce into the skin to administer insulin in a minimally invasive and targeted manner (*6*). Previous works associated with insulin-based MN systems mainly focused on bolus insulin delivery without delaying or prolonging the dissolution or absorption of insulin (*7*). Nevertheless, the sustained or kinetically controlled delivery is more preferable than bolus insulin delivery and is essential to fulfill the full potential of transdermal delivery for maintaining drug concentrations within a therapeutic range over a predetermined period of time (*8*). Research in this field is directed in the main to develop various types of microneedle systems including hollow microneedles (*9*), biodegradable microneedles (*10*) as well as swelling microneedles (*11*) to achieve controllable insulin delivery. These attempts are inspiring for diabetes management, but it will be much more meaningful if a single MN patch incorporates basal-bolus regimen that enables constant basal insulin supply and on-demand bolus dosing to achieve a better match of prandial insulin use to meal consumption and glucose uptake patterns.

Related studies have begun to explore the combination of MNs and iontophoresis patches/infusion pump for simultaneous delivery of fast-acting and long-acting insulin (*12*). However, the complex applicator device constrains the transformation convenience and increases financial burdens. In addition, smart insulin-based MN patches embedding glucose-responsive materials have also been investigated for closed-loop diabetes therapeutics (*13*, *14*). In recent years, we have used the hydrogels to the rapidly separating MN platforms for controlled transdermal insulin delivery (*15*). On the basis of insulin-loaded hydrogel MNs mounted on a corresponding supporting MN array, the novel device enables us to fully insert the upper hydrogel MN into the skin within seconds and subsequently provides controlled insulin release over a tunable period to manage blood glucose levels.

Here, we extend substantially the previous findings with rapidly separating hydrogel MN system by demonstrating the design of a single insulin-loaded MN patch that enables mimicking a near-normal physiological pattern of insulin secretion. Given these objectives, we designed two parallel approaches for fabrication of integrated MN patches (IMPs) containing three compartments for independently controlling the kinetics of insulin during transdermal application. These three divided compartments can be composed of either (i) different matrix materials [e.g., gelatin (Gel), cross-linked Gel (cGel), and cGel/hyaluronic acid particulate mixture (cGel-cHA)] or (ii) different types of insulin (e.g., short-, intermediate-, and long-acting insulin) to obtain basal-bolus insulin therapy to cover the postprandial glycemic excursions, thereby achieving daily persistent glycemic control in a single MN patch (Fig. 1). We conclude that the integrated MN designs can not only rapidly respond to elevated glucose levels but also provide the ability for rapid transdermal delivery of controlled

Beijing Laboratory of Biomedical Materials, College of Materials Science and Engineering, Beijing University of Chemical Technology, Beijing 100029, P. R. China.
*Corresponding author. Email: xdguo@buct.edu.cn

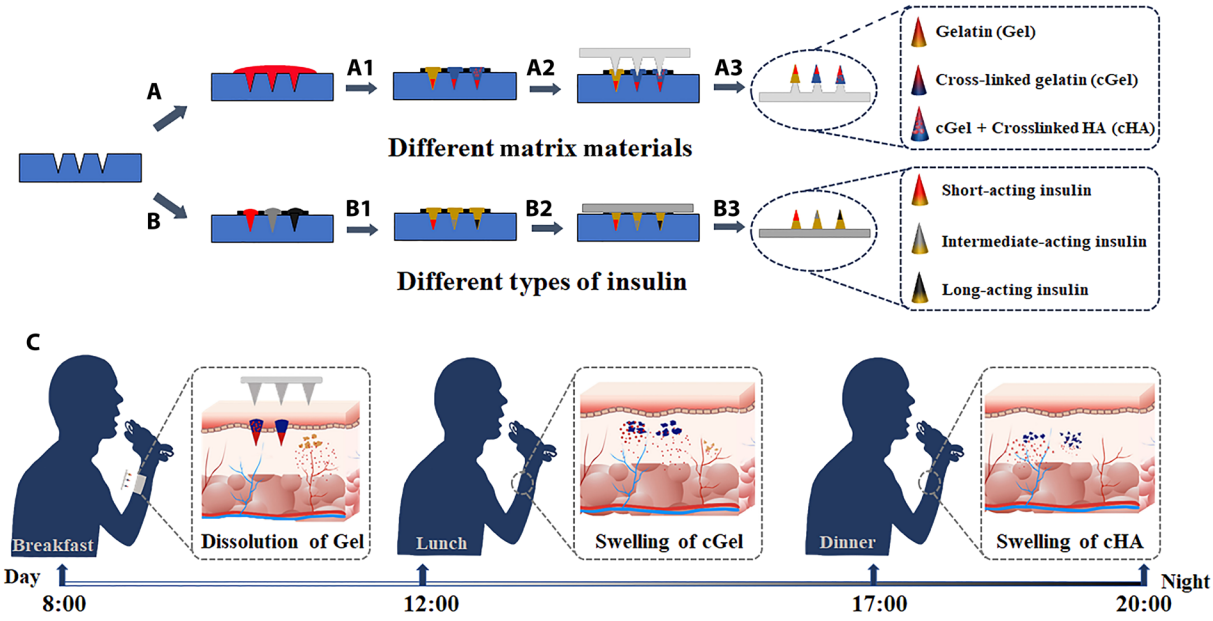

Fig. 1. Fabrication process and insulin release principle of the IMP. (**A**) Polydimethylsiloxane (PDMS) molds were first filled with regular insulin under vacuum. (A1) Different polymer solutions (Gel, cGel, and cGel-cHA) were separately applied to this insulin-loaded mold. (A2) Corresponding PLA MN patch was aligned to the mold cavities. (A3) The IMP fabricated from different matrix materials was detached from the mold after overnight drying. (**B**) PDMS molds were separately filled with different types of (short-, intermediate-, and long-acting) insulin under vacuum. (B1) The Gel solution was cast onto the insulin-loaded mold. (B2) A base plate was pasted on the filled mold. (B3) The IMP loaded with different types of insulin was removed from PDMS mold after drying. (**C**) Schematic of the insulin release principle (rapid insulin release caused by dissolution of Gel, sustained insulin/insulin-loaded cHA particulate release with the swelling of the cGel matrix, and relative slow insulin release with the swelling of cHA particulates) of the IMP to achieve a thrice-daily insulin supplement (timed with meals) after administration.

release depots for basal-bolus combinatorial release of insulin to improve intraday postprandial glucose control.

RESULTS AND DISCUSSION

Synthesis and characterization of MN matrix materials

To fabricate insulin-loaded IMP system capable of both bolus and sustained combinatorial release of insulin to satisfy the human physiological demands for insulin, both the native and cross-linked polymers (Gel and HA) were applied to serve as the matrix materials of the IMP in the study. To our knowledge, Gel and HA are U.S. Food and Drug Administration–approved naturally occurring biomaterials with a degradation pathway that is well understood (*16*). However, the comparatively higher hydrophilicity makes them inappropriate to be used for controlled drug release system. Therefore, changing the materials' hydrophilicity represents a worthy direction to pursue. In this context, the biopolymer composites of genipin-cGel and 1,4-butanediol diglycidyl ether (BDDE)–cHA were synthesized for MN production to achieve flexibility for tuning the kinetics of insulin release in the skin. BDDE is the cross-linker that exhibited negligible cytotoxicity and has been applied in most of the market-leading HA fillers (*17*), while the biological cross-linking agent of genipin, extracted from gardenia fruits, is superior to many other synthetic cross-linking agents as it is 10,000 times less toxic than aldehyde and epoxy cross-linkers (*18*).

In this work, the hydrogels of cHA and cGel were produced through aqueous solution polymerization, with gelation initiated at room temperature to avoid insulin devitalization. The resultant hydrogels yielded microporous and interconnected morphology structures, as shown in the cross-sectional scanning electron microscopy (SEM) images (Fig. 2A), with the microstructures being more prominent in the treatment of cross-linking agents. In contrast, the native hydrogels exhibited irregular pore size distribution and appeared with some collapses, which may lead to weakened mechanical strength. The noticeable difference in ^{1}H nuclear magnetic resonance (NMR) and Fourier transform infrared (FT-IR) spectra of HA before and after cross-linking with BDDE confirmed chemical reactions that occurred to the native HA structure (Fig. 2, B and C). NMR results revealed two new distinctive signals at 1.8 and 1.5 parts per million (ppm) in the cHA sample, which can be attributed to the unsaturated bond in the unsaturated disaccharide and the $-CH_2$ group of the BDDE molecule, respectively (*19*). Integration of the signal at 1.5 ppm with regard to the peak at 1.9 ppm (*N*-acetyl groups) showed approximately 7.6% degree of modification in the prepared cHA sample. Spectra of FT-IR showed a larger downward peak at 2920 cm^{-1} (C—H stretching) and a new emerging peak at 1260 cm^{-1} (ether linkage) in the cHA sample, presumably due to the cross-linking reaction between the epoxide groups of BDDE and the hydroxyl groups of HA (fig. S1) (*20*). In addition, the degradation ratio of the cHA was notably lower compared to the native HA (Fig. 2D), indicating that the cross-linked polymer matrix can slow down enzymatic invasion and increase the duration of hydrogel residence. Together, these results confirmed that the cross-linking process plays a critical role in producing HA-based MNs for controlling drug delivery.

With respect to cGel, the ninhydrin assay determined that the cross-linking degree between genipin and Gel increased over time and reached stable value (approximately 60%) in 24 hours (Fig. 2E). After treatment with genipin solution, Gel chains were chemically cross-linked via the formation of an aldehyde group, which is

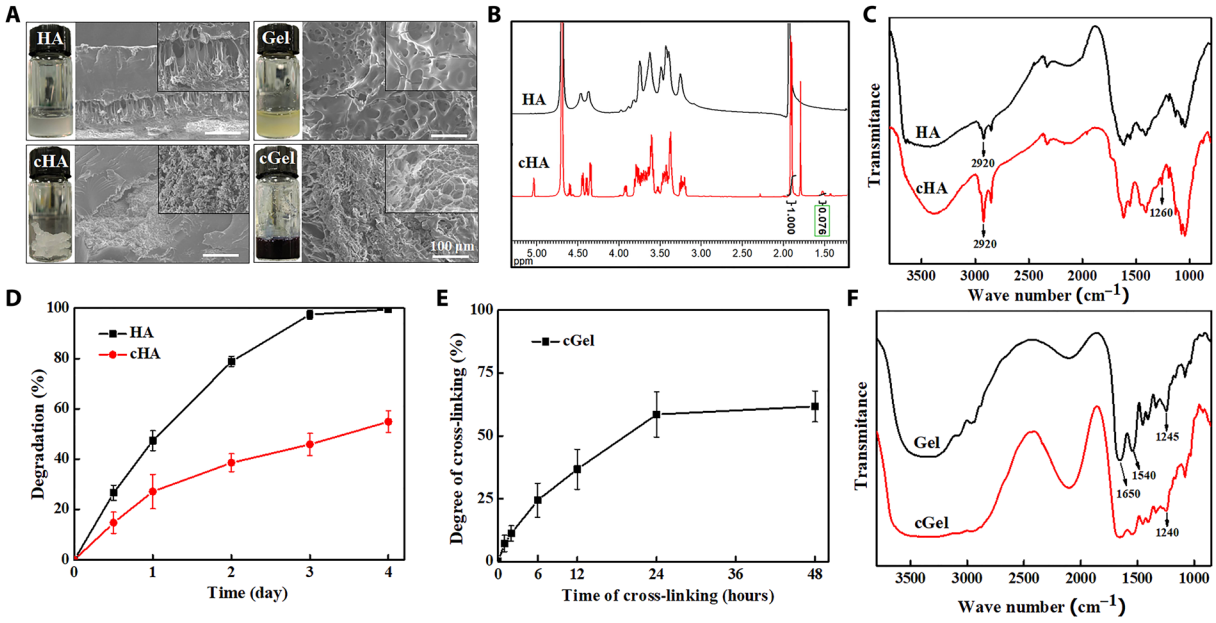

Fig. 2. Characterization of the MN matrix materials. (**A**) Macroscopic appearance and SEM images of HA, Gel, cHA, and cGel. (Inset) Zoomed-in images of the materials. (**B**) ^{1}H NMR spectra of HA and cHA digested fragments. (**C**) FT-IR spectra of HA and cHA. (**D**) Degradation profiles of HA and cHA with hyaluronidase. (**E**) Degree of cross-linking (%) of Gel solution in function of cross-linking time. (**F**) FT-IR spectra of Gel and cGel. Error bars indicate SD ($n = 3$). Photo credit for (A): Bozhi Chen, Beijing University of Chemical Technology.

manifested in the dark blue macroscopic appearance of the cGel (fig. S2) (*18*). It was revealed that the genipin molecule undergoes a nucleophilic attack by the primary amines of Gel, followed by a nucleophilic substitution on the ester groups to form cross-linked networks (fig. S3) (*21*). As presented in the FT-IR spectra (Fig. 2F), the characteristic peaks observed at 1245, 1540, and 1650 cm^{-1} in the Gel sample are assigned to C═O bands of carbonyl groups, N─H band of the amino group, and N─H bands of the amide III group, respectively (*22*). Specifically, the intensity of N─H band of the amino group decreased, and the peak lightly shifted toward the lower wave number (1245 to 1240 cm^{-1}) was observed in the cGel sample, which can be attributed to the cross-linking reactions between genipin and amino groups on Gel (*23*). It can be expected that the cross-linking process was sufficient to form a compact network, potentially acting in a physicochemical manner to prolong the release of the insulin.

Design and fabrication of integrated MN patch

Clinical practices have demonstrated that thrice-daily insulin supplement (timed with meals) provides effective postprandial glucose control and can efficiently prevent or delay diabetic complications (*24*). Guided by this, we combined rapidly separating technique with multiple individual MN arrays on a single MN patch, which would provide rapid administration through brief MN application while enabling independently controlled insulin release from the deposited polymer MNs within the skin (Fig. 3A). The resulting IMP comprised three individual 3 × 9 array of MNs in a single patch, and each needle consists of a 550-μm-long MN mounted on a corresponding polyvinyl alcohol (PVA)–coated polylactic acid (PLA) supporting array, with an exposed length of 200 μm and an overlap of approximately 350 μm (Fig. 3B). This mosaic structure was found to be critical to counteract skin deformation during the insertion process, and the soluble PVA coating layer speeds up the separation of PLA supporting array and the hydrogel MNs (*25*). Notably, the MNs were of consistent microstructures and highly reflected the dimensions of the polydimethylsiloxane (PDMS) mold. We hypothesize that such a device has potential to serve as an alternative to daily multiple insulin injections due to its ability to independently control the insulin release rate and to co-deliver multiple types of insulin in a single patch.

We previously demonstrated that cGel MNs penetrate the skin and maintain insulin concentrations within therapeutic levels over 5 hours, and previous work has also shown the ability of cHA particulates to be prepared into MNs and is more resistive to dissolution (*19*, *26*). Combining the merits of cGel and cHA, we here developed cGel-cHA MNs with a composite structure for further controlled transdermal insulin-release rate. In this case, fluorescent signal from the entrapped fluorescein isothiocyanate (FITC)–labeled cHA particulates was localized at the tip or upper portion of the needle, whereas the cGel alone formed the outer layer of the MNs (Fig. 3C). We hypothesized that cGel-cHA MNs are strong enough for reliable skin insertion (Fig. 3D, step 1), and the upper drug-loaded MNs were rapidly separated from the PLA supporting array and embedded in the subcutaneous tissue due to the dissolution of the interfacial PVA coating layer and mechanical separation (Fig. 3D, step 2). This would then lead to the swelling and disintegration of the outer cGel layer, letting both the encapsulated drug and drug-loaded cHA particulates to slowly seep through the cross-linked polymer matrix for either bolus or sustained combinatorial release of drug molecules (Fig. 3D, step 3). The ratio of cHA particulates entrapped in MNs ultimately influences the mechanical strength of the needle due to the discontinuity of each composition materials. In this context, cHA particulates were screened with a 300-mesh sieve (GB/T6003.2012) and mixed with cGel solution in various ratios of 80:20, 60:40, 40:60, 20:80, and 0:100 (Fig. 3E). The successful application of cGel-cHA MNs was evaluated by inserting MNs with different cHA contents

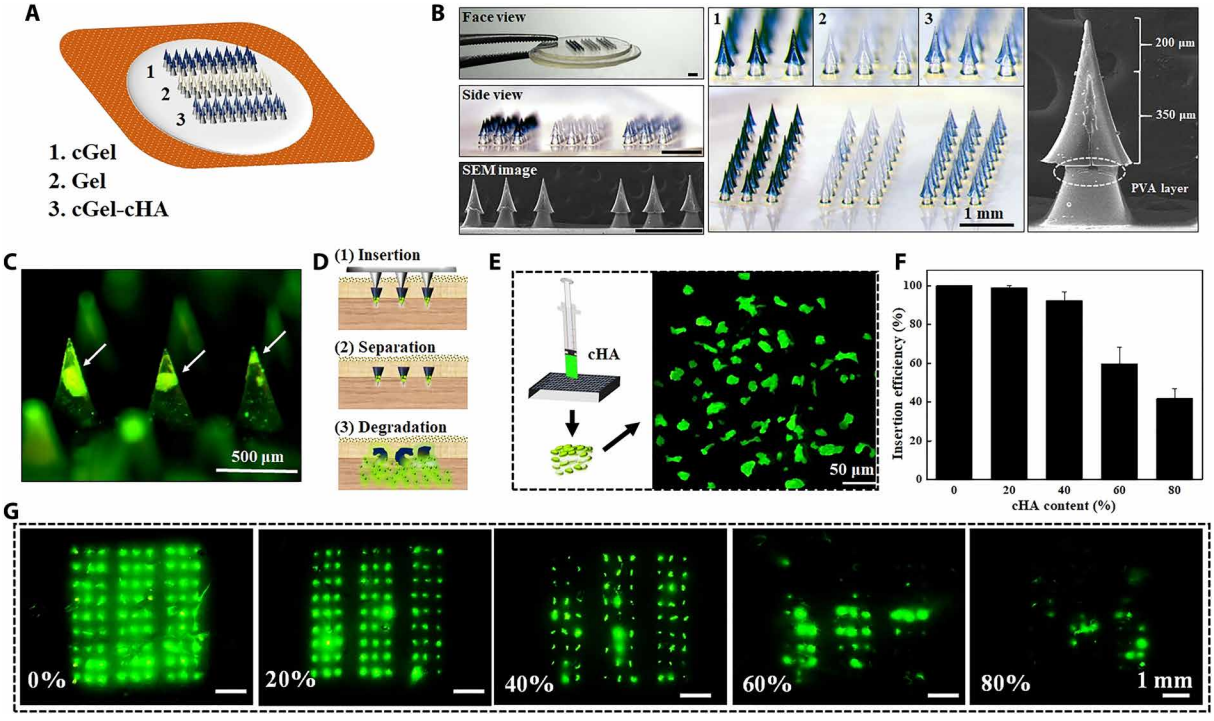

Fig. 3. Design and analysis of the IMP. (**A**) Illustration of the integrated MN patch. (**B**) Morphology of the fabricated IMP imaged by optical microscopy and SEM. (**C**) Fluorescence image of the cGel-cHA MNs, showing the encapsulation of cHA particulates (green color) in the needle. (**D**) cGel-cHA MN delivery scheme. (1) An MN patch is inserted into the skin. (2) The patch is rapidly separated, allowing drug-loaded MNs to embed into the skin. (3) cGel layer swelled and released both the encapsulated drug and cHA particulates for sustained release of drug molecules. (**E**) Schematic illustration of the pulverization of cHA hydrogel. (**F**) Skin insertion efficiency of the cGel-cHA MNs as a function of cHA content. Data represent average ± SD ($n = 3$ replicates). (**G**) Corresponding fluorescence images of the porcine skin after removal of cGel-cHA MNs with different cHA contents. Photo credit for (B): Bozhi Chen, Beijing University of Chemical Technology.

into porcine skin. It is evident from the results that increasing the cHA content substantially decreased the skin insertion success rate, and the cGel MNs with 60% cHA content were inserted only partially over the array of MNs (Fig. 3F). FITC was more quickly diffused through the skin from the native cGel MNs (0% cHA content), as evidenced by the diffusion of the green fluorescence around insertion sites (Fig. 3G), indicating that the drug release rate can be manipulated by controlling the selection of drug carrier and encapsulation modes. Together, cGel MNs with approximately 40% content of cHA particulates were appropriate for this study in consideration of the marginal safety of the mechanical strength of MNs and their drug release kinetics.

Characterization of integrated MN patch

Stronger polymer MNs could be advantageous for transdermal drug delivery in tougher tissue sites of the body, while weak mechanical behavior limits the usage of MN-based systems (*27*). To this end, mechanical properties of the fabricated MNs, including the fracture strength and insertion ability, were analyzed by applying axial compression load to the MNs and by inserting the MNs into Parafilm M films and animal skins with a definite force generated by a force test bench. In literature reports, Parafilm M films have been widely used for mechanical testing as a standard routine quality control method (*28*). The force-displacement curve of cGel-cHA MNs exhibited an initial increase in applied force with displacement, followed by a sudden drop at the local maximum of the force curve that indicated the failure force (Fig. 4A), which could possibly be due to the encapsulation of cHA particulates in the hydrogel MNs. In contrast to cGel-cHA MNs, the other MNs did not show a distinct transition point during the compressing test, indicating that the hard compression causes only progressive deformation of the MNs. However, the fabricated MN patches were all capable of piercing the model membranes, as evidenced by the holes created in each layer of the membrane and the insertion depth calculated by the pierced layers (Fig. 4B and fig. S4). The upper drug-loaded MNs were effectively detached from the supporting array and embedded onto the parafilm immediately after insertion, which was consistent with the expected effect (Fig. 4C). Guided by these results, we next applied the IMP on both the porcine and living mouse skin to further confirm the preclinical effects of the patch. As expected, application of MNs created indelible puncturing sites on the skin surface and penetration cavities (~300 μm) inside the epidermis layer (Fig. 4, D and E), confirming that the fabricated IMP was well penetrated and completely deposited within the tissue. The difference between the insertion depth and the length of the MNs can be attributed to the highly viscoelastic nature of the skin (*29*). Moreover, after MN separation, there were little residual materials in the supporting patch, further evidencing the efficient delivery of upper drug-loaded MNs into the skin. Subsequent transepidermal water loss (TWEL) measurements indicated that the micro-holes created by the IMP were greatly resealed around 5 hours after removal of the patch, as evidenced by the TWEL value considerably increasing immediately after treatment and recovering to a level similar to the control group without MN treatment (Fig. 4F). This may be attributed to the minimally invasive nature of the MNs

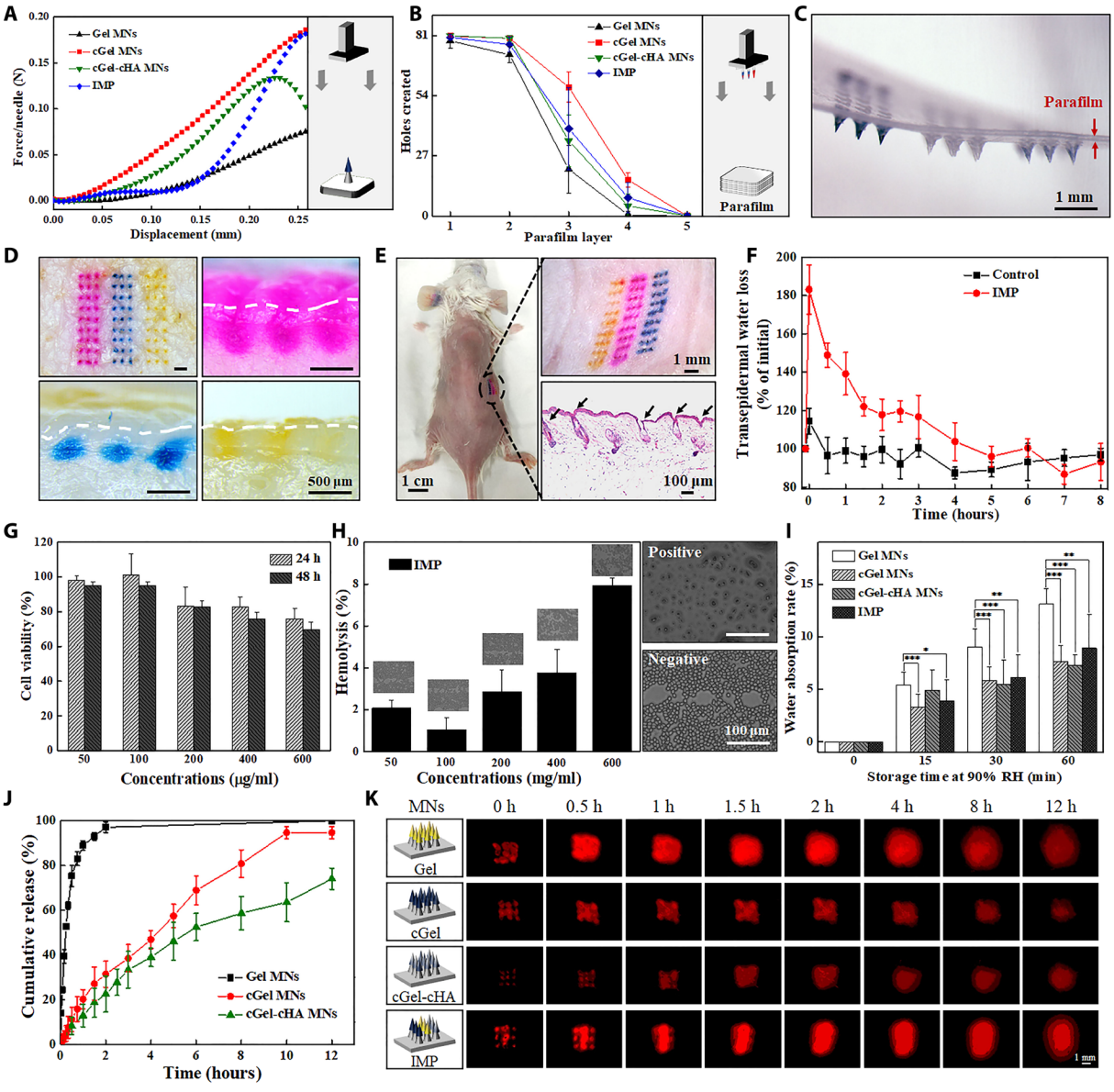

Fig. 4. Characterization of the fabricated MN patch. (**A**) Typical force-displacement curve of the compression force of different material-based MNs. (Inset) Schematic illustration of the used setup. (**B**) Holes created in each parafilm layer after insertion of the MN patch using constant 5 N of compression force ($n = 5$). (**C**) Corresponding photograph of the first parafilm layer after removal of the supporting array. (**D**) Porcine cadaver skin after treatment with IMP (top left) and its corresponding histological sections penetrated by Gel MNs (top right), by cGel MNs (bottom left), and by cGel-cHA MNs (bottom right). The white dashed lines indicate the skin surface. (**E**) Mouse dorsum after treatment with an IMP and its corresponding histological section (bottom right). (**F**) TWEL values of mice skin at different time points after an IMP application ($n = 5$). (**G**) Relative viability of L-929 cells incubated with various concentrations of the IMP after 24 and 48 hours, respectively ($n = 3$). (**H**) Hemolysis assay results for the IMP. (Inset) Corresponding microscopic images of red blood cells with and without exposure ($n = 3$). (**I**) Hygroscopic analysis of the fabricated MNs at 90% RH atmosphere with different storage time. Asterisk indicates a significant difference (Student's t test, $^*P < 0.05$, $^{**}P < 0.01$, and $^{***}P < 0.001$) ($n = 8$). (**J**) In vitro release profiles of insulin from the fabricated MNs in phosphate buffer (37°C) ($n = 4$). (**K**) Schematic illustration of the fabricated MNs, and real-time release of sulforhodamine B (red color) onto the porcine cadaver skin surface (0 to 12 hours). Photo credit for (C) to (E): Bozhi Chen, Beijing University of Chemical Technology.

and the spontaneous healing of the skin tissue. Together, these lines of evidence indicated that the fabricated IMP was strong enough for successful skin insertion, easy to detach from the supporting array immediately after application, and well tolerated without causing obvious adverse effects on the skin.

Given the promising mechanical properties, we next sought to investigate the biocompatibility of the IMP by cytotoxicity and hemolysis tests. Overall, the fabricated IMP exhibited high biocompatibility because cell viability persisted more than 80% after exposure to various concentrations of MN extracts for 24 and 48 hours (Fig. 4G). In addition, blood compatibility was examined by measuring the lysis of erythrocyte cells after incubation with the fabricated IMP. Consistent with the cell viability evidence, no extensive morphological alterations of the erythrocytes were detected, and the percentage hemolysis was below the hemolytic threshold of erythrocytes [≤10% (*30*)] in all tested groups (Fig. 4H). The negligible

cytotoxicity and hemolysis of the IMP are probably attributed to the biocompatibility of the matrix materials (native and cross-linked Gel and HA), which can be degraded into harmless by-products or into by-products that are identical to substances already found in body tissue (*17*).

A prominent advantage involved to the proposed IMP is that it allows simple tuning of release kinetics through the incorporation of multiple individual arrays in a single MN patch. Thus, the water resistance of the proposed MN patch was evaluated to explain its hygroscopy and prolonged release kinetics by exposing MNs to high moisture condition [at a relative humidity (RH) of 90%]. We defined the water absorption rate at 0 before storage, and the increase of water absorption rate indicates the absorption of moisture from the wet environment. Because of the increase of water content level, the matrix materials of the MNs dissolved or swelled, resulting in the discharge of the encapsulated molecules. As expected, the water absorption rates of these MNs were increased over time, and especially, the native Gel MNs showed more sensitive response to the high humidity condition than the other kinds of MNs (Fig. 4I), suggesting that the cross-linking of the MNs plays a critical role in controlling the release kinetics. This could be explained by the formulation of the polymer network, which impedes the diffusion of moisture molecules, thereby improving the stability of the MNs. In vitro insulin release from these three individual MNs was determined by using an in-house–designed dialysis system, which permitted only insulin to pass through the membrane (fig. S5). Compared to cross-linked polymer–based MNs, the Gel MNs released ≥80% of the insulin in the first 0.5 hours of application and nearly 100% within 2 hours, indicating that the release pattern largely depended on the dissolution of the matrix material (Fig. 4J). In contrast, prolonged-release profiles were observed for insulin encapsulated in cross-linked MNs because the molecules can only diffuse with the swelling of the cross-linked polymer matrix. It should also be noted that the cGel-cHA MNs exhibited slower release kinetics after 5 hours of exposure, which can be attributed to the fact that the swelling of outer cGel layer leads to quick discharge of both insulin molecules and insulin-loaded cHA particulates within the first 5 hours, whereas the cHA particulates subsequently swell slowly, letting the insulin gradually diffuse through the interwoven meshwork.

The real-time release profiles of the MNs in porcine skin further demonstrate that the IMP was capable of both rapid and sustained combinatorial release of therapeutics, as evidenced by the drug (red in color) diffused through the skin with different rates (Fig. 4K). It is assumed that the processes of drug release from the integrated MNs mainly include (i) rapid release with the dissolution of Gel, (ii) release with the swelling or dissolution of the cGel matrix, and (iii) slow release after overcoming the barrier of cGel and cHA matrix. These results were consistent with the previous water resistance and cumulative release tests already discussed and together demonstrate the successful combination of various release kinetics in a single MN patch.

In vivo studies of the fabricated MNs for diabetes treatment

To verify the therapeutic efficacy of the prepared insulin-loaded MNs, the streptozotocin (STZ)–induced diabetic rats (~220 mg of body weight) were selected to treat with a variety of MN samples: regular insulin–loaded MNs fabricated from different polymers (Gel, cGel, and cGel-cHA), different types of insulin-loaded Gel MNs (short-, intermediate-, and long-acting insulin), and sham patches (control). The insulin dose in each MN patch was controlled to a target content of 0.3 IU by using different concentrations of insulin solution during the manufacturing process, as determined by reversed-phase high-performance liquid chromatography (HPLC) method (fig. S6). The HPLC chromatogram of insulin release from the prepared MNs showed that, except for solvent peaks, only one peak was attributed to insulin, preliminarily indicating that there was no any detectable degradation of insulin in these insulin-loaded MNs. In addition, the blood glucose levels of treated rats were monitored over a span of 12 hours, and the effectiveness of different MN patches for real-time insulin release is directly reflected by the hypoglycemic effect (*31*). Of note, the blood glucose levels in the control group fluctuated slightly within the first 8 hours of treatment, followed by a ~20% decline in the later 4 hours, suggesting that the long-time fasting could affect the level of blood glucose (Fig. 5, A and B). In contrast, the prepared insulin-loaded MN patch had a notable effect on diabetes, as evidenced by the satisfactory blood glucose control. The data indicated that the insulin release kinetics can be simply tuned by changing either the matrix materials or insulin species. However, it should also be noted that both the intermediate- and long-acting insulin have a certain risk of causing hypoglycemia with the same insulin dose. We thus hypothesize that a basal-bolus combinatorial insulin delivery system could be a tremendous potential to mitigate the risk of hypoglycemia and improve daily persistent glycemic control.

In this context, the proposed IMP, which comprises a basal-bolus regimen, was inserted into the shaven dorsal skin of the rats by using a homemade applicator and removed after 2 min. Blank IMP (without insulin) and a dose-matched subcutaneous insulin injection were also applied to the diabetic rats for comparison purpose. As expected, rats treated with regular insulin (0.3 IU) delivered through subcutaneous injection led to ~75% decline in blood glucose within 1.5 hours and subsequently quickly reverted to the initial level at 4 hours, whereas the glucose levels for administration via the IMP declined gently and maintained a long-term euglycemia (Fig. 5C). It is clear that the controlled-release characteristic of IMP is exclusively due to the obstruction effect of cross-linked polymers matrix (*32*, *33*). Correspondingly, plasma insulin measurement by enzyme-linked immunosorbent assay (ELISA) method further revealed continuous replenishment of insulin under IMP treatment, as opposed to faster absorption and shorter efficacy time of the subcutaneous injection (Fig. 5D). Among the tested rats, the area under the curve (AUC) values were comparable to those injected with insulin solution (218.37 ± 4.47 μU hours/ml) to those inserted with insulin-loaded IMP (161.28 ± 25.92 μU hours/ml) (Table 1). The subcutaneous injection led to a sharp insulin increase, reaching a peak concentration (C_{max} = 121.64 ± 22.86 μU/ml) at 1 hour after treatment, and then markedly dropped to negligible levels within 4 hours. In the case of IMP treatment, the plasma insulin concentration increased gradually up to maximal level (37.56 ± 9.17 μU/ml) at T_{max} (2.67 ± 0.58 hours) and fluctuated between 5 and 16 μU/ml within the time frame. These results confirm that insulin administrated via IMP was almost completely absorbed from the skin into the systemic circulation, and the biological activity of released insulin remained intact after exposing to the matrix materials of the MNs. Further analysis of the plasma insulin profiles demonstrated that the IMP was associated with a longer mean residence time (MRT) (4.88 ± 0.30 hours) than insulin injection formulation (1.47 ± 0.26 hours), suggesting not only that IMP was prolonged blood glucose control but also that

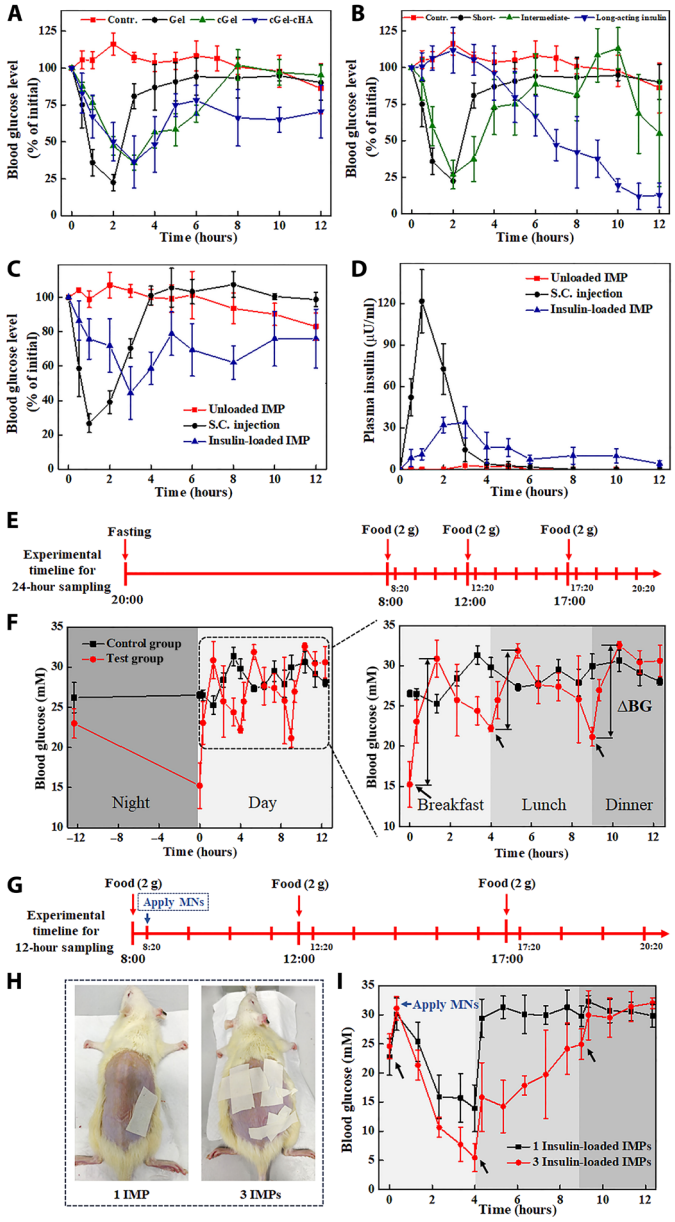

Fig. 5. In vivo studies of the fabricated MNs for diabetes treatment. Blood glucose levels in diabetic rats after treatment with (**A**) regular insulin–loaded MNs fabricated from different materials and (**B**) different types of insulin-loaded Gel MNs. Effects of various application methods of insulin on (**C**) blood glucose levels and (**D**) plasma insulin concentrations in diabetic rats. (**E**) Experimental timeline. (**F**) Blood glucose changes in diabetic rats received food ad libitum (control) and standardized breakfast-lunch-dinner feeding patterns. Blood glucose excursion (ΔBG) was significantly higher at the first feeding of the day than at the other times. (**G**) Timeline. (**H**) Rat dorsum inserted with one and three patches of the insulin-loaded IMP, respectively. (**I**) Blood glucose levels in diabetic rats after treatment with different numbers of the IMP. S.C., subcutaneous. Photo credit for (H): Bozhi Chen, Beijing University of Chemical Technology.

it could also efficiently minimize excessive fluctuations and the risk of hypoglycemia.

Most previous experience with insulin dosage regimens has involved on-demand bolus dosing to lower blood glucose, with limited work to further study the intraday variability of postprandial blood glucose (*1*). Guided by this, here, we investigated the characteristics of glucose fluctuations in diabetic rats and assessed the advantages of IMP for attenuating the postprandial glycemic excursion and improving durable efficacy of the antidiabetic therapy. In brief, the rats with blood glucose stabilized around 25 mM were grouped to provide three daily standardized meals at a comparatively fixed time after 12 hours of overnight fasting (Fig. 5E), whereas rats with water and food ad libitum throughout the study were subjected as control group. The data showed that the overall blood glucose swings with food intake, and for the same food intake, the peak blood glucose excursion (ΔBG) after breakfast was greater than after both lunch and dinner (Fig. 5F), which was likely associated with the dysregulation of the normal circadian hormonal patterns (*34*). In addition, the experimental rats displayed more obvious intraday glucose fluctuations and nocturnal hypoglycemia compared to the control rats, indicating that the diabetics with a traditional breakfast-lunch-dinner feeding pattern are even more in need of timely insulin supplement to avoid intermittent high blood glucose exposure.

Extensive clinical trials have confirmed that the frequent or large glycemic fluctuations have deleterious effects on diabetes complications, thus making control of glycemic variability essential (*35*, *36*). In addition to lifestyle intervention, insulin-loaded IMP with multiple release kinetics may have potential applicability in reducing postprandial glycemia oscillations and the frequency of episodes of hyperglycemia, thereby preventing later complications in diabetes. To highlight this feature, the diabetic rats received three daily meals at a comparatively fixed time and separately attached with one and three regular insulin–loaded IMP immediately after breakfast (Fig. 5, G and H). In agreement with previous observation (*37*), the rats treated with varying insulin doses exhibited dose-dependent hypoglycemic effect, as a further reduction of blood glucose levels was observed when the amount of MN patch increased from one to three (Fig. 5I). Application of insulin-loaded IMP triggered a notable blood glucose decline with no appreciable lag time, which could be explained by the near-instantaneous dissolution of the Gel MNs on hydration by interstitial fluid in skin and a relatively large amount of insulin absorbed on the surface of the integrated MNs. Nonetheless, the blood glucose level in rats treated with one IMP quickly rebounded to the hyperglycemia state after a meal, whereas those given three IMPs showed a lower spike in blood glucose after meal and maintained a normoglycemic state over a comparatively long time, reflecting the better synchronization of insulin release profiles and food absorption. Furthermore, the insulin doses adequate to counteract meal consumption and cover the postprandial glycemic excursions would also be critical to sustaining the duration of therapeutic effects. Together, these results support the notion that a single MN patch is capable of combinatorial bolus and sustained insulin delivery for mealtime insulin needs.

CONCLUSIONS

In summary, we designed and fabricated an integrated MN patch composed of a basal-bolus insulin regimen, which enables percutaneous delivery of insulin with multiphasic release kinetics to best cover the postprandial glycemic excursions, thus improving intraday glucose fluctuations and preventing complications. Both the artificial membranes and biological tissue tests demonstrated the rapid and efficient transdermal drug delivery capability of the proposed MNs, and no dermatosis-related effects were observed on the MN-treated

Table 1. Pharmacokinetic parameters following subcutaneous injection of insulin (0.3 U) and administration of insulin-loaded integrated MNs (0.3 U) in diabetic rats. Results are expressed as the mean ± SE of at least three experiments.

Group	AUC_{0_12} (μU hour/ml)	C_{max} (μU hour/ml)	MRT_{0_12} (hours)	T_{max} (hours)
Subcutaneous injection	218.37 ± 4.47	121.64 ± 22.86	1.47 ± 0.26	1.00 ± 0.00
Integrated MNs	161.28 ± 25.92	37.56 ± 9.17	4.88 ± 0.30	2.67 ± 0.58

sites. Moreover, the hypoglycemic experiments in rats indicated that the integrated MNs not only enable reduced postprandial glycemia oscillations but also prolong the duration of therapeutic effects. This work is the first investigation of the relationship between postprandial blood glucose excursion and food intake in diabetics treated with MN-based system, providing new information to research the feasibility of integrated MN patch to serve as an alternative to a multiple-dose injection therapy. Aside from delivery of the insulin with multiple kinetics, the modularity and integrability of this MN patch suggest its potential to sequentially release different drugs for synergistic therapy.

MATERIALS AND METHODS

Materials

PDMS (Sylgard 184) was obtained from Dow Corning (Midland, USA). PLA was purchased from Lakeshore Biomaterials Inc. (AL, USA). Cell counting kit (CCK-8) and STZ were purchased from AbMole BioScience (TX, USA). Gel (from cold water fish skin and from porcine skin), FITC, phosphate buffer, and deuterium oxide (D_2O, $D > 99.9\%$) were purchased from Sigma-Aldrich (MO, USA). Ehrlich's reagent was purchased from BioTechnology Co Ltd. (Shanghai, China). Acetic acid, sodium carbonate anhydrous (Na_2CO_3), and dibasic sodium phosphate (Na_2HPO_4) were obtained from Sinopharm Chemical Reagent Co Ltd. (Beijing, China). Insulin (short-, intermediate-, and long-acting types) was purchased from Wanbang Biopharmaceuticals Co. Ltd. (Jiangsu, China). HA ($M_w \approx 350{,}000$ Da) was purchased from Toronto Research Chemicals Inc. (Toronto, Canada). BDDE ($M_w = 202.25$ Da) was purchased from Adamas Reagent Co. Ltd. (Basel, Switzerland). Genipin was purchased from J&K Scientific (Beijing, China). Mouse fibroblast cell lines (L-929 cells) were purchased from iCell Bioscience (Shanghai, China), and female Balb/c mice were obtained from the Institute of Laboratory Animal Sciences (Beijing, China). Aqueous solutions were carried out using ultrapure water from a reverse osmosis membrane system, unless otherwise stated.

Preparation of MN matrix materials and drug formulations

The cGel solutions and cHA particulates were prepared for encapsulation of drugs by a blending cross-linking process according to our previously reported methods (*19*, *26*). Briefly, Gel powders were dissolved in ultrapure water under magnetic stirring at room temperature to produce 40% (w/v) homogeneous solution. Next, the genipin solution was mixed in the produced Gel solution [0.36% (w/v) of genipin] for 96 hours to produce the cGel. The cHA hydrogel was prepared by mixing HA powders and BDDE into 0.25 M NaOH (pH 13) at room temperature for 2 hours and, after that, by purifying with 95% ethanol. The cHA hydrogel particulates with a diameter of less than 50 μm were collected by grinding, squeezing, and filtering processes. To make cHA-cGel solution, the obtained cHA particulates were first immersed into drug solution to produce drug-loaded particulates. Then, the particulate suspension and cGel solution were fully mixed with a stirrer to obtain the cHA-cGel solution. In this study, the insulin solution was prepared using 15 mg of insulin powders dissolved in 1 ml of 0.01 M HCl solution, and the insulin-cHA particulates were formulated with target drug contents of 5 weight % on the basis of the therapeutic efficacy. Sulforhodamine B/FITC drug powders were separately dissolved in ultrapure water to serve as model drug solutions.

Fabrication of the integrated MN patch

IMPs containing different matrix materials or diverse types of insulin were fabricated by a two-step vacuum casting procedure involving a PDMS mold. Initially, the supporting PLA MNs were first fabricated using hot pressure method and then coated with PVA solution by a dip-coating process (*25*). A modified casting process that involved vacuum molding was applied to prepare the upper drug-loaded MNs. Approximately 0.1 ml of the prepared drug solution, as the first layer, was poured onto the mold and degassed using a vacuum to drive the solution into cavities. Following removal of residual drugs from the mold surface, the prepared matrix materials (Gel, cGel, and cGel-cHA) were separately smeared on the drug-loaded mold and store in a vacuum for 45 min at −90 kPa to properly fill the mold cavities. Next, tailor-made pasters were attached to the filled mold to not only divide the whole MN patch into three divided compartments but also keep the overlaps between upper drug-loaded MNs and PLA supporting MNs. The solid supporting MNs were then aligned manually toward the mold cavities to ensure adhesion of drug-loaded MNs onto the PLA MNs. The solidified drug-loaded MN patches were successfully detached from the mold after overnight drying at room temperature and used for further analysis. For MN patches encapsulating diverse types of insulin, tailor-made pasters were attached to the PDMS mold and the insulin (short-, intermediate-, and long-acting) solution was separately loaded into the created three divided compartments using a vacuum process. The homogeneous Gel solution was then spread on the filled mold and dried overnight to form the MN patch, containing three types of insulin.

Mechanical and insertion properties of the prepared MNs

A motorized displacement-force test bench (ESM301, Mark-10, Force Gauge Model, USA) was used to determine the mechanical and insertion properties of the IMP, as described in our previous study (*32*). For the compression test, the prepared MNs were compressed between two metallic parallel plates in a vertical direction. The detailed process includes the following steps: (i) A 3 × (3 × 9) array containing 81 MNs was vertically attached to the flat stainless-steel station, and (ii) an axial force was applied to move the force

probe to press the MNs at a speed of 1.1 mm/s until a preset maximum load (20 N) was reached. The axial force was recorded for the movement of the probe as a displacement function. The successive increase in application force caused deformation or breakage in the MNs, and the stage was withdrawn at several points during the test to understand the failure mode of MNs.

With regard to insertion tests, the fabricated MNs were separately inserted into artificial membranes and biological tissues with a definite force (10 N) were generated by the test bench. Before penetration test, hairs of the skin were carefully removed using a disposable shaver and the Parafilm M film was folded into an eight-layer sheet (~1 mm thickness) to achieve the thickness similarity to human skin (*28*). Following attachment of the MN patch to the force sensors, the MNs were vertically pressed into the Parafilm M sheet and animal skins, respectively. After separation, the sheet was unfolded to evaluate the number of holes left in each layer and to further identify the detached MNs embedded in the parafilm. The puncture marks on the skin surface were also imaged under bright-field microscopy (SZX7, Olympus, Tokyo, Japan) to ascertain the insertion ratio. For histological analysis, skin samples were sliced from the middle of needle holes to determine the insertion depth and drug release location.

Measurement of TWEL

To further determine the successful insertion of the IMP and skin recovery characteristic after application, TWEL values were measured using a digital moisture monitor (SK-IV, Facecaie, Guangdong, China) at mice skin sites with and without (control) MN treatment. The back skin of mice was shaved 24 hours before skin insertion test, and only the skins without signs of illness were selected for the following treatment. The MNs were kept under ultraviolet (UV) light for 15 min to sterilize the needle and applied into the disinfected skin with a constant force of 10 N. TWEL values were recorded before and directly after removing MN patch and repeated at the preset time points according to the manufacturer's instructions.

Biocompatibility of the prepared MNs

Cytotoxicity of the IMP toward L-929 fibroblast cell lines was analyzed by CCK-8 assay (*26*). In detail, L-929 cells were cultured in 96-well plates at a density of 1.0×10^4 cells per well in 100 μl of Dulbecco's modified Eagle's medium (DMEM) (containing 10% fetal bovine serum and 1% penicillin-streptomycin). The plates were next inoculated in a humidified incubator (37°C, 5% CO_2) for 12 hours before addition of serial dilutions of the dissolved MN solution. After 24-hour incubation, the culture medium was replaced with fresh matching medium containing CCK-8 reagent (0.1 ml) for an additional 2 hours. Calculating the final absorbance at 450 nm determined the relative cell survival percentages using a microplate reader (EnSpire, PerkinElmer, MA, USA). Cells cultured in the initial medium were regarded as negative control.

Hemolytic activity of the IMP was assessed by measuring the lysis of erythrocytes as a consequence of disruption in the cellular membrane caused by the exposure to the prepared MNs. Briefly, the intact erythrocytes were washed with phosphate-buffered saline (PBS) twice and incubated with MNs at various concentrations from 50 to 600 μg/ml at 37°C. PBS reagent and Triton X-100 [0.2% (v/v)] were used as negative (0% hemolysis) and positive (100% hemolysis) controls in this study, respectively. After 1-hour incubation, the tested samples were centrifuged at 3000 rpm for 20 min to collect the supernatant. Testing the optical density (OD) value at 540 nm determined the lysis of erythrocytes using a UV-visible spectrophotometer (UV-2600, Shimadzu Corporation, Japan). The blood samples from tested groups were photographed using a fluorescence microscope (EVOS FL Cell Imaging System, Life Technologies, Paisley, UK) to evaluate the morphological changes in erythrocytes.

Hygroscopy of the prepared MNs

The hygroscopic analysis of MNs regarding different matrix materials was ascertained under high moisture conditions. Briefly, the prepared MN patches were kept in a desiccator for 48 hours, and then samples were stored in a constant humidity chamber (HWS-70B, Taisite Instrument Co. Ltd., Tianjin, China) at 25°C with 90% RH. The water absorption of MN samples was calculated by measuring the weight of pre- and post-incubated MN samples at predetermined times (*38*).

In vitro controlled drug release test

To differentiate the dissolution and release kinetics of insulin loaded in three different materials (Gel, cGel, and cGel-cHA), in vitro insulin release experiments were performed by loading insulin-loaded MNs fabricated from different materials into a dialysis bag (molecular weight cutoff, 10,000; Jinsui Bio-Technology, Shanghai, China), as described previously (*26*). The membrane molecular weight cutoff was chosen on the basis of insulin molecular weight. In detail, the MN-loaded dialysis bag was completely soaked in 0.01 M phosphate buffer with continuous stirring at 360 rpm and maintained at 37°C for the entire duration of the analysis. To determine the insulin release from the prepared MNs, approximately 300 μl of samples was taken at preset time points and supplemented with an equal volume of fresh medium. The actual concentration of insulin in each of the obtained samples was quantified by HPLC assay as follows (*39*): The samples were filtered and injected into an HPLC system (Elite 230II, with a P 230II pump and UV 230II detector; Elite Analytical Instruments Co. Ltd., Dalian, China). The analysis was performed by reversed-phase HPLC at 214 nm using a C18 column (Supersil ODS2, 5 μm, 4.6 × 200 mm, Elite Analytical Instruments Co. Ltd., China), mobile phase consisting of 0.1 M KH_2PO_4 buffer:acetonitrile: methanol [62:26:12 (v/v)], and a flow rate of 1.0 ml/min. Every sample was loaded in triplicate, and the averaged reading was taken for further quantification.

To achieve real-time visualization of drug releases from the prepared MNs within the skin, 3 × 3 arrays of sulforhodamine B–loaded MNs were applied on the porcine cadaver skin and continuously monitored under a fluorescence microscope (SZX7, Olympus, Tokyo, Japan). The skin samples were kept in a suitable humidity condition to prevent skin dehydration throughout the study. To better parallel the drug delivery kinetics of the MNs, drug diffusion region was imaged using identical exposure conditions and processed by an image processing application to obtain a clearer vision (*40*).

In vivo studies of the prepared MNs for diabetes treatment

Animal studies were approved by the institutional animal care committee of China-Japan Friendship Hospital. Female Balb/c mice (~15 to 20 g) and Sprague-Dawley rats (~200 to 250 g) obtained from the Institute of Laboratory Animal Sciences (Beijing, China) were acclimatized to standard laboratory conditions for more than 2 weeks before any experiments.

After overnight fasting, rats were made diabetic by intraperitoneal injection of STZ (100 mg/kg body weight) dissolved in 0.2 ml of

sodium citrate buffer solution (pH 4.5, 0.05 M). The blood glucose levels of the treated rats were monitored using a OneTouch glucometer (LifeScan Inc., Milpitas, CA, USA) for 1 week until stabilized, and only the animals with blood glucose levels above 16.7 mM (300 mg/dl) were defined as diabetic and used in this study. Before experimentation, diabetic rats were anesthetized using isoflurane and their back hair was gently shaved. The prepared MN patches, with or without insulin (0.3 IU) loaded, were inserted into the dorsal skin by using a homemade applicator and removed after 2 min. As control experiments, a similar dose of insulin solution was administered subcutaneously with a hypodermic needle. The blood samples were obtained from the cut tips of the tail at selected time points after treatment (from 0 to 12 hours), and the blood glucose levels versus time were determined using a glucometer, as previously described. In some cases, the obtained blood samples were centrifuged at 4400 rpm for 10 min to collect plasma, which was then stored frozen (−20°C) until analysis using an Insulin ELISA kit (Meimian Biotech, Yancheng, China) to measure plasma levels of insulin delivered to the rats.

To study the postprandial glycemic excursions following three daily standardized solid mixed meal (breakfast, lunch, and dinner), the diabetic rats with blood glucose stabilized around 25 mM received a strict dietary control. After a 12-hour overnight fast, diabetic rats were admitted to the meal between 8:00 a.m. and 8:20 a.m. in the morning, 12:00 a.m. and 12:20 p.m. on the afternoon, and 17:00 p.m. and 17:20 p.m. on the evening of the study. The test meal contained predominantly rapidly absorbed carbohydrates (standard 2 g; approximately 70:15:15 carbohydrate:protein:fat ratio). As control experiments, the diabetic rats were acclimatized to laboratory conditions with water and food ad libitum at 12-hour light/dark cycle throughout the study. Immediately before initiation of the meal (0 hour) and at selected times after the meal began, blood samples were collected from the cut tips of the tail to measure the blood glucose concentrations. To further evaluate the pharmacokinetics and efficacy of the insulin-loaded integrated MNs in daily postprandial glucose control, the diabetic rats were separately given one and three IMPs at once. Samples for blood glucose monitoring were collected at 20 min before MN application and thereafter at 1-hour intervals for 12 hours.

Statistical analysis

All analyses were conducted with a sample size of $n \geq 3$. The data were analyzed using Excel and Origin 8.5. Descriptive statistics were expressed as mean values ± SE. Student's t test was used for comparisons between data points. The statistical differences were assumed to be reproducible when $P < 0.05$.

SUPPLEMENTARY MATERIALS

Supplementary material for this article is available at http://advances.sciencemag.org/cgi/content/full/6/28/eaba7260/DC1

REFERENCES AND NOTES

1. X. Jin, D. D. Zhu, B. Z. Chen, M. Ashfaq, X. D. Guo, Insulin delivery systems combined with microneedle technology. *Adv. Drug Deliv. Rev.* **127**, 119–137 (2018).
2. G. M. Reaven, Role of insulin resistance in human disease. *Diabetes* **37**, 1595–1607 (1988).
3. J. Arya, M. R. Prausnitz, Microneedle patches for vaccination in developing countries. *J. Control. Release* **240**, 135–141 (2016).
4. E.-S. Khafagy, M. Morishita, Y. Onuki, K. Takayama, Current challenges in non-invasive insulin delivery systems: A comparative review. *Adv. Drug Deliv. Rev.* **59**, 1521–1546 (2007).
5. D. R. Owens, B. Zinman, G. Bolli, Alternative routes of insulin delivery. *Diabetic Med.* **20**, 886–898 (2003).
6. P. C. DeMuth, J. J. Moon, H. Suh, P. T. Hammond, D. J. Irvine, Releasable layer-by-layer assembly of stabilized lipid nanocapsules on microneedles for enhanced transcutaneous vaccine delivery. *ACS Nano* **6**, 8041–8051 (2012).
7. J. J. Norman, M. R. Brown, N. A. Raviele, M. R. Prausnitz, E. I. Felner, Faster pharmacokinetics and increased patient acceptance of intradermal insulin delivery using a single hollow microneedle in children and adolescents with type 1 diabetes. *Pediatr. Diabetes* **14**, 459–465 (2013).
8. P. C. DeMuth, W. F. Garcia-Beltran, M. L. Ai-Ling, P. T. Hammond, D. J. Irvine, Composite dissolving microneedles for coordinated control of antigen and adjuvant delivery kinetics in transcutaneous vaccination. *Adv. Funct. Mater.* **23**, 161–172 (2013).
9. S. P. Davis, W. Martanto, M. G. Allen, M. R. Prausnitz, Hollow metal microneedles for insulin delivery to diabetic rats. *IEEE Trans. Biomed. Eng.* **52**, 909–915 (2005).
10. N. Hosseini-Nassab, D. Samanta, Y. Abdolazimi, J. P. Annes, R. N. Zare, Electrically controlled release of insulin using polypyrrole nanoparticles. *Nanoscale* **9**, 143–149 (2017).
11. R. F. Donnelly, T. R. Singh, M. J. Garland, K. Migalska, R. Majithiya, C. M. McCrudden, P. L. Kole, T. M. Mahmood, H. O. McCarthy, A. D. Woolfson, Hydrogel-forming microneedle arrays for enhanced transdermal drug delivery. *Adv. Funct. Mater.* **22**, 4879–4890 (2012).
12. C. J. Rini, E. McVey, D. Sutter, S. Keith, H.-J. Kurth, L. Nosek, C. Kapitza, K. Rebrin, L. Hirsch, R. J. Pettis, Intradermal insulin infusion achieves faster insulin action than subcutaneous infusion for 3-day wear. *Drug Delivery Transl. Res.* **5**, 332–345 (2015).
13. J. Yu, Y. Zhang, Y. Ye, R. DiSanto, W. Sun, D. Ranson, F. S. Ligler, J. B. Buse, Z. Gu, Microneedle-array patches loaded with hypoxia-sensitive vesicles provide fast glucose-responsive insulin delivery. *Proc. Natl. Acad. Sci. U.S.A.* **112**, 8260–8265 (2015).
14. J. C. Yu, Y. Q. Zhang, W. J. Sun, A. R. Kahkoska, J. Q. Wang, J. B. Buse, Z. Gu, Insulin-responsive glucagon delivery for prevention of hypoglycemia. *Small* **13**, 5 (2017).
15. D. D. Zhu, B. Z. Chen, M. C. He, X. D. Guo, Structural optimization of rapidly separating microneedles for efficient drug delivery. *J. Ind. Eng. Chem.* **51**, 178–184 (2017).
16. T. J. Hinton, Q. Jallerat, R. N. Palchesko, J. H. Park, M. S. Grodzicki, H.-J. Shue, M. H. Ramadan, A. R. Hudson, A. W. Feinberg, Three-dimensional printing of complex biological structures by freeform reversible embedding of suspended hydrogels. *Sci. Adv.* **1**, e1500758 (2015).
17. K. De Boulle, R. Glogau, T. Kono, M. Nathan, A. Tezel, J. X. Roca-Martinez, S. Paliwal, D. Stroumpoulis, A review of the metabolism of 1,4-butanediol diglycidyl ether-crosslinked hyaluronic acid dermal fillers. *Dermatol. Surg.* **39**, 1758–1766 (2013).
18. K. De Clercq, C. Schelfhout, M. Bracke, O. De Wever, M. Van Bockstal, W. Ceelen, J. P. Remon, C. Vervaet, Genipin-crosslinked gelatin microspheres as a strategy to prevent postsurgical peritoneal adhesions: In vitro and in vivo characterization. *Biomaterials* **96**, 33–46 (2016).
19. J. N. Zhang, B. Z. Chen, M. Ashfaq, X. P. Zhang, X. D. Guo, Development of a BDDE-crosslinked hyaluronic acid based microneedles patch as a dermal filler for anti-ageing treatment. *J. Ind. Eng. Chem.* **65**, 363–369 (2018).
20. M. Al-Sibani, A. Al-Harrasi, R. H. Neubert, Study of the effect of mixing approach on cross-linking efficiency of hyaluronic acid-based hydrogel cross-linked with 1,4-butanediol diglycidyl ether. *Eur. J. Pharm. Biopharm.* **91**, 131–137 (2016).
21. L. Solorio, C. Zwolinski, A. W. Lund, M. J. Farrell, J. P. Stegemann, Gelatin microspheres crosslinked with genipin for local delivery of growth factors. *J. Tissue Eng. Regen. Med.* **4**, 514–523 (2010).
22. Y. Zhang, Q. S. Wang, K. Yan, Y. Qi, G. F. Wang, Y. L. Cui, Preparation, characterization, and evaluation of genipin crosslinked chitosan/gelatin three-dimensional scaffolds for liver tissue engineering applications. *J. Biomed. Mater. Res. A* **104**, 1863–1870 (2016).
23. S. P. Mallick, S. S. Sagiri, V. K. Singh, B. Behera, A. Thirugnanam, D. K. Pradhan, M. K. Bhattacharya, K. Pal, Genipin-crosslinked gelatin-based emulgels: An insight into the thermal, mechanical, and electrical studies. *AAPS PharmSciTech* **16**, 1254–1262 (2015).
24. T. Heise, L. Nosek, C. Roepstorff, S. Chenji, O. Klein, H. Haahr, Distinct prandial and basal glucose-lowering effects of insulin degludec/insulin aspart (IDegAsp) at steady state in subjects with type 1 diabetes mellitus. *Diabetes Ther.* **5**, 255–265 (2014).
25. M. C. Chen, S. F. Huang, K. Y. Lai, M. H. Ling, Fully embeddable chitosan microneedles as a sustained release depot for intradermal vaccination. *Biomaterials* **34**, 3077–3086 (2013).
26. B. Z. Chen, M. Ashfaq, D. D. Zhu, X. P. Zhang, X. D. Guo, Controlled delivery of insulin using rapidly separating microneedles fabricated from genipin-crosslinked gelatin. *Macromol. Rapid Commun.* **39**, 1800075 (2018).
27. J. Tang, J. Wang, K. Huang, Y. Ye, T. Su, L. Qiao, M. T. Hensley, T. G. Caranasos, J. Zhang, Z. Gu, K. Cheng, Cardiac cell–integrated microneedle patch for treating myocardial infarction. *Sci. Adv.* **4**, eaat9365 (2018).
28. L. K. Vora, R. F. Donnelly, E. Larraneta, P. Gonzalez-Vazquez, R. R. S. Thakur, P. R. Vavia, Novel bilayer dissolving microneedle arrays with concentrated PLGA nanomicroparticles for targeted intradermal delivery: Proof of concept. *J. Control. Release* **265**, 93–101 (2017).
29. M. G. An, H. P. Liu, Dissolving microneedle arrays for transdermal delivery of amphiphilic vaccines. *Small* **13**, 8 (2017).

30. M. Ashfaq, N. Verma, S. Khan, Highly effective Cu/Zn-carbon micro/nanofiber-polymer nanocomposite-based wound dressing biomaterial against the *P. aeruginosa* multi- and extensively drug-resistant strains. *Mater. Sci. Eng. C* **77**, 630–641 (2017).
31. Q. Peng, X. Sun, T. Gong, C. Y. Wu, T. Zhang, J. Tan, Z. R. Zhang, Injectable and biodegradable thermosensitive hydrogels loaded with PHBHHx nanoparticles for the sustained and controlled release of insulin. *Acta Biomater.* **9**, 5063–5069 (2013).
32. B. Z. Chen, Y. Yang, B. B. Wang, M. Ashfaq, X. D. Guo, Self-implanted tiny needles as alternative to traditional parenteral administrations for controlled transdermal drug delivery. *Int. J. Pharm.* **556**, 338–348 (2019).
33. A. Than, C. Liu, H. Chang, P. K. Duong, C. M. G. Cheung, C. Xu, X. Wang, P. Chen, Self-implantable double-layered micro-drug-reservoirs for efficient and controlled ocular drug delivery. *Nat. Commun.* **9**, 4433 (2018).
34. S. Franc, D. Dardari, C. Peschard, J.-P. Riveline, M. Biedzinski, B. Boucherie, C. Petit, E. Requeda, F. Mistretta, M. Varroud-Vial, G. Charpentier, Can postprandial blood glucose excursion be predicted in type 2 diabetes? *Diabetes Care* **33**, 1913–1918 (2010).
35. C. Wang, L. Lv, Y. Yang, D. Chen, G. Liu, L. Chen, Y. Song, L. He, X. Li, H. Tian, W. Jia, X. Ran, Glucose fluctuations in subjects with normal glucose tolerance, impaired glucose regulation and newly diagnosed type 2 diabetes mellitus. *Clin. Endocrinol.* **76**, 810–815 (2012).
36. J. Wang, J. Yu, Y. Zhang, X. Zhang, A. R. Kahkoska, G. Chen, Z. Wang, W. Sun, L. Cai, Z. Chen, C. Qian, Q. Shen, A. Khademhosseini, J. B. Buse, Z. Gu, Charge-switchable polymeric complex for glucose-responsive insulin delivery in mice and pigs. *Sci. Adv.* **5**, eaaw4357 (2019).
37. Y. Ito, E. Hagiwara, A. Saeki, N. Sugioka, K. Takada, Feasibility of microneedles for percutaneous absorption of insulin. *Eur. J. Pharm. Sci.* **29**, 82–88 (2006).
38. M. C. He, B. Z. Chen, M. Ashfaq, X. D. Guo, Assessment of mechanical stability of rapidly separating microneedles for transdermal drug delivery. *Drug Deliv. Transl. Res.* **8**, 1034–1042 (2018).
39. A. Najjar, M. Alawi, N. AbuHeshmeh, A. Sallam, A rapid, isocratic HPLC method for determination of insulin and its degradation product. *Adv. Pharm.* **2014**, 6 (2014).
40. M. Kim, B. Jung, J. H. Park, Hydrogel swelling as a trigger to release biodegradable polymer microneedles in skin. *Biomaterials* **33**, 668–678 (2012).

Acknowledgments
Funding: This work was financially supported by the National Natural Science Foundation of China (51873015 and 51673019) and the long-term subsidy mechanism from the Ministry of Finance and the Ministry of Education of PRC. **Author contributions:** B.Z.C. and Y.Y.X. performed experimental measurements. B.Z.C. and L.Q.Z. drafted the paper. B.Z.C. and X.P.Z. contributed to the data interpretation. X.D.G. directed the research and provided financial support. **Competing interests:** The authors declare that they have no competing interests. **Data and materials availability:** All data needed to evaluate the conclusions in the paper are present in the paper and/or the Supplementary Materials. Additional data related to this paper may be requested from the authors.

Submitted 2 January 2020
Accepted 27 May 2020
Published 10 July 2020
10.1126/sciadv.aba7260

Citation: B. Z. Chen, L. Q. Zhang, Y. Y. Xia, X. P. Zhang, X. D. Guo, A basal-bolus insulin regimen integrated microneedle patch for intraday postprandial glucose control. *Sci. Adv.* **6**, eaba7260 (2020).

ScienceAdvances

A basal-bolus insulin regimen integrated microneedle patch for intraday postprandial glucose control

Bo Zhi ChenLi Qin ZhangYi Yun XiaXiao Peng ZhangXin Dong Guo

Sci. Adv., 6 (28), eaba7260. • DOI: 10.1126/sciadv.aba7260

Science Advances (ISSN 2375-2548) is published by the American Association for the Advancement of Science. 1200 New York Avenue NW, Washington, DC 20005. The title *Science Advances* is a registered trademark of AAAS.